



Article

The Mean Moment of Inertia for Irregularly Shaped Phobos and Its Application to the Constraint for the Two-Layer Interior Structure for the Martian Moon

Zhen Zhong ^{1,*} , Qilin Wen ¹, Jianguo Yan ² and Lijun Pang ¹

¹ School of Physics and Electronic Science, Guizhou Normal University, Guiyang 550025, China; qlwen1541@gznu.edu.cn (Q.W.); pangli@gznu.edu.cn (L.P.)

² State Key Laboratory of Information Engineering in Surveying, Mapping and Remote Sensing, Wuhan University, Wuhan 430079, China; jgyan@whu.edu.cn

* Correspondence: zzhong@gznu.edu.cn

Abstract: The interior structure of Phobos has been the subject of debate in recent years, with the moment of inertia being a determining factor. To study this structure, we modeled Phobos with a two-layer structure and calculated its mean density and moment of inertia using updated gravity coefficients of degree-2 and forced libration amplitudes. By minimizing the misfit between modeled and derived moment of inertia, and observed and modeled mean density, we determined the frequency distribution for estimated parameters, including the core radius r_c , core density ρ_c , and density ρ_m of the outer layer. Our results indicate that the optimized core radius is around 8.2 km for our models, along with a core density compromise of approximately $2500 \text{ kg}\cdot\text{m}^{-3}$, and an outer layer density of around $1400 \text{ kg}\cdot\text{m}^{-3}$. These values have remarkable sensitivity to the misfit function, implying a higher density likely inside Phobos compared to the outer layer. Given that the large core density was associated with ice content, it suggested that the fractional ice content in the outer layer is approximately 11% with a rock density of $2200 \text{ kg}\cdot\text{m}^{-3}$, while the content in the core is lower at 2.4% with a rock density of $3000 \text{ kg}\cdot\text{m}^{-3}$. The methodology introduced in this study can be further used to study the interior structure of irregularly shaped asteroids.



Citation: Zhong, Z.; Wen, Q.; Yan, J.; Pang, L. The Mean Moment of Inertia for Irregularly Shaped Phobos and Its Application to the Constraint for the Two-Layer Interior Structure for the Martian Moon. *Remote Sens.* **2023**, *15*, 3162. <https://doi.org/10.3390/rs15123162>

Academic Editor: Giancarlo Bellucci

Received: 22 April 2023

Revised: 31 May 2023

Accepted: 10 June 2023

Published: 17 June 2023



Copyright: © 2023 by the authors. Licensee MDPI, Basel, Switzerland. This article is an open access article distributed under the terms and conditions of the Creative Commons Attribution (CC BY) license (<https://creativecommons.org/licenses/by/4.0/>).

Keywords: moment of inertia; mean density; two-layer interior structure; irregular shape; Phobos

1. Introduction

Phobos is a natural satellite of Mars and is the larger of the two Martian satellites, with Deimos being the smaller one. Phobos has an irregularly shaped surface with a mean radius close to 11 km, as reported by Willner et al. [1]. Phobos' surface is heavily cratered, with many craters spread over its surface, likely suggesting its feature of a relatively old satellite [2]. The dominant feature of the body is Stickney, which is the largest crater on the moon with a diameter of approximately 9.5 km [3]. The origin of Phobos and its composition are not yet fully understood [4,5]. It likely originated from a recycling process in which the progenitors from the impacting process perhaps were destroyed into a Roche interior ring and re-accreted several times [6]. To understand the formation of Phobos, it is crucial to examine its interior structure. By analyzing its structure, we can gain insight into its origin and evolutionary history.

While radar data can provide some information on the interior structure of Phobos, a direct exploration of the moon is crucial to accurately determine its moment of inertia. The moment of inertia is closely related to the density distribution inside Phobos. However, there has been no direct measurement of Phobos, except for a few measurements obtained during flybys of orbiters approaching Mars. As a result, the interior structure of Phobos remains an open issue. To determine the origin of Phobos, the Japan Aerospace Exploration Agency (JAXA) plans to carry out a direct survey of the Martian Moons eXploration (MMX)

mission in 2024 [7,8]. Prior to the MMX mission, numerous studies attempted to detect the interior structure of Phobos [1,4,9–12]. Recently, Le Maistre et al. [13] investigated the likely interior structure of Phobos by analyzing its tidal response to Mars, while Dmitrovskii et al. [14] attempted to study this subject by analyzing the tidal bulge height.

In addition to the research mentioned above, another way to explore the interior structure of Phobos is to consider its mean density and moment of inertia. This approach was used in the past by Sohl et al. [15] to determine the composition and structure of the Martian interior. Their method involved modeling both the moment of inertia and bulk density of the nearly spherical Mars. By comparing the difference between the observed and modeled moment of inertia and the misfit between the observed and modeled mean density, they were able to estimate the density distribution as well as the interior structure of Mars. Yan et al. [16] used a similar method to identify the size and composition of the lunar core. Based on the precession rate from InSight [17], we recently used a similar method to investigate the potential size and density of the Martian inner core [18]. Similarly, this method could be applied to small celestial bodies by estimating the mean density and moment of inertia and comparing them with modeled values. However, it should be noted that this approach is quite challenging for small celestial bodies with irregular shapes, such as asteroids and moons of planets. Most small bodies in the real world are irregularly shaped and do not achieve quasi-hydrostatic equilibrium. Therefore, the method proposed by Sohl et al. [15] needs to be updated to include the case of irregular shapes.

We thus deduced an expression to calculate the moment of inertia and mean density for bodies with irregular shapes. Using the updated method, we estimated the likely structure of Phobos by considering the recent degree-2 gravity coefficients as well as the forced libration amplitude of Phobos. The updated gravity coefficients of degree-2 were derived from MEX Doppler-tracking data by Yang et al. [19]. The forced libration amplitudes of Phobos were updated in recent studies by Burmeister et al. [12] and Lainey et al. [11]. We used these updated values of degree-2 gravity coefficients and libration amplitudes to deduce the moment of inertia for Phobos. By comparing this deduced value and our modeled moments of inertia, we can gain insight into the distribution of mass and the interior structure of Phobos. Due to the lack of information on Phobos' interior structure, it has been previously assumed to be homogeneous. However, other models have proposed a multilayer structure based on density and forced libration observations [10] or a rubble pile composition that includes voids and/or water ice [1,19–21].

To validate our method, the interior structure of Phobos was modeled here as a two-layered structure with varying densities. The positive density gradient in our study indicates that the density of the core was greater than that of the outer layer. Conversely, the negative gradient suggests that the density of the core was lower than that of the outer layer. If Phobos had multiple layers inside, then the density distribution inside the moon would be continuous, and the estimated densities of the two-layer model would be represented as mean values. Additionally, an approximate zero density gradient indicates a homogeneous interior structure within Phobos. The two-layer model discussed here is thus applicable in cases where a density gradient exists and can account for the case where Phobos has a continuous density distribution. This paper is structured as follows. In Section 2, we present two models, each consisting of two layers. In Section 3, we describe our methodology of the moment of inertia and misfit function. In Sections 4 and 5, we present the results and discussion. Finally, Section 6 summarizes the conclusions.

2. Shape of Phobos and Its Two-Layer Model

The Phobos shape model was first derived as an ellipsoidal model by Thomas in 1989 [22]. Then, Simonelli et al. [23] generated a shape model with 2×2 degree grid spacing. Using image data from the European Mars Express Mission, Willner et al. [10] derived a shape model expanded with a spherical harmonic function close to degree and order 17. Subsequently, Willner et al. [1] used stereo images from Mars Express and Viking Orbiter to derive a global digital terrain model (DTM) with 100 m/pixel resolution.

This DTM is widely used in Phobos gravity forward modeling and surface properties research [13,19,24,25]. The DTM derived by Willner et al. [1], which is available online [26], is shown in Figure 1. Phobos is tidally locked to Mars, which means that the same side of Phobos always faces Mars. This side is known as the sub-Mars side, which is shown in Figure 1a. The leading side of Phobos is the side that faces forward in its orbit around Mars, in the direction of its movement. This side of Phobos is displayed in Figure 1b.

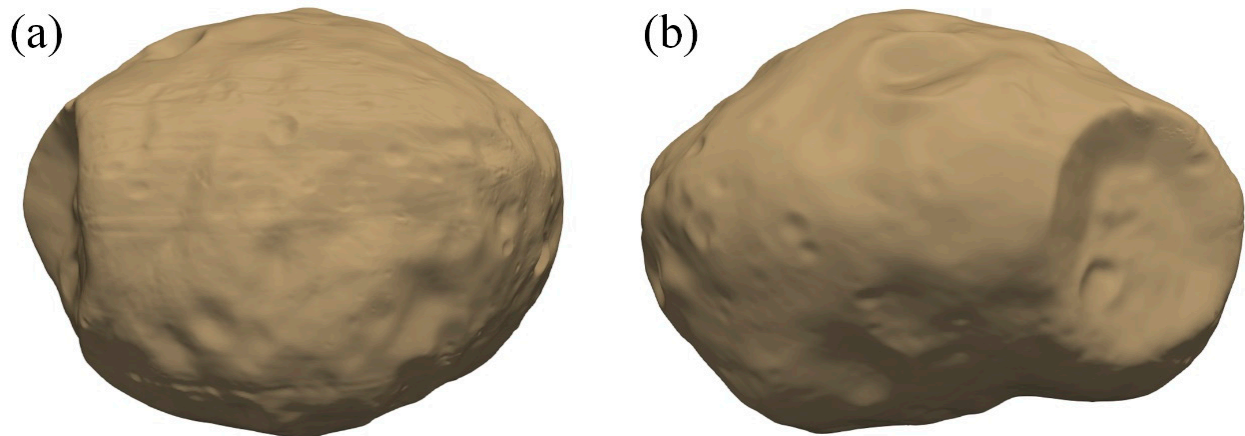


Figure 1. Shape of Phobos. (a) shows the sub-Mars side, and (b) displays the leading side of Phobos.

Recent studies on the interior structure of Phobos have considered the possibility that the density of its interior may vary with depth [13,14,27]. Studies have also suggested that a two-layer model, with a solid core and an outer layer composed of rock and ice, is appropriate to explain the gravity coefficients of low degrees [21,28]. We opted for a two-layer model when estimating Phobos' internal structure for several reasons. Firstly, the limited constraint information available for Phobos makes multi-layer models highly uncertain. Secondly, given the small volume of Phobos, it is unlikely that large-scale differentiation processes occurred in its interior. Finally, we accounted for Phobos' irregular shape when calculating its mean moment of inertia. Models with more than three layers would increase complexity and hinder the estimation of model parameters. Therefore, based on these considerations, we only used a two-layer model to estimate Phobos' mean moment of inertia. The two-layer models are shown in Figure 2. Our two-layer model assumed that Phobos is composed of an inner solid core with a density of ρ_c , and an outer layer that is likely a mixture of rock and ice with a density of ρ_m . The black areas in the diagrams represent the solid cores, while the areas between the red outer shapes and the black areas represent the outer layers. Figure 2a shows Model-I with a spherical core, which is commonly considered a simplified internal structure of celestial bodies. Figure 2b displays Model-II with an irregularly shaped core that has a shape similar to the surface of Phobos. This model considers the core's irregular shape to result from impacts or other geological processes. We used r_c here as the radius of the core of Model-I in Figure 2a and considered the same sign as the mean radius of the core of Model-II in Figure 2b. It should be noted that the difference between the core density ρ_c and the density of the outer layer ρ_m cannot fully prove the differentiation of Phobos. An alternative possibility is that Phobos has a continuous density distribution, where the density gradually changes from the core to the outer layer. In the case of a continuous density distribution, the estimated density of the core ρ_c and the density ρ_m of the outer layer would be mean values, and the corresponding radius of the core r_c would also be a mean value. This means that there would not be a sharp boundary between the core and the outer layer, but instead a gradual transition zone.

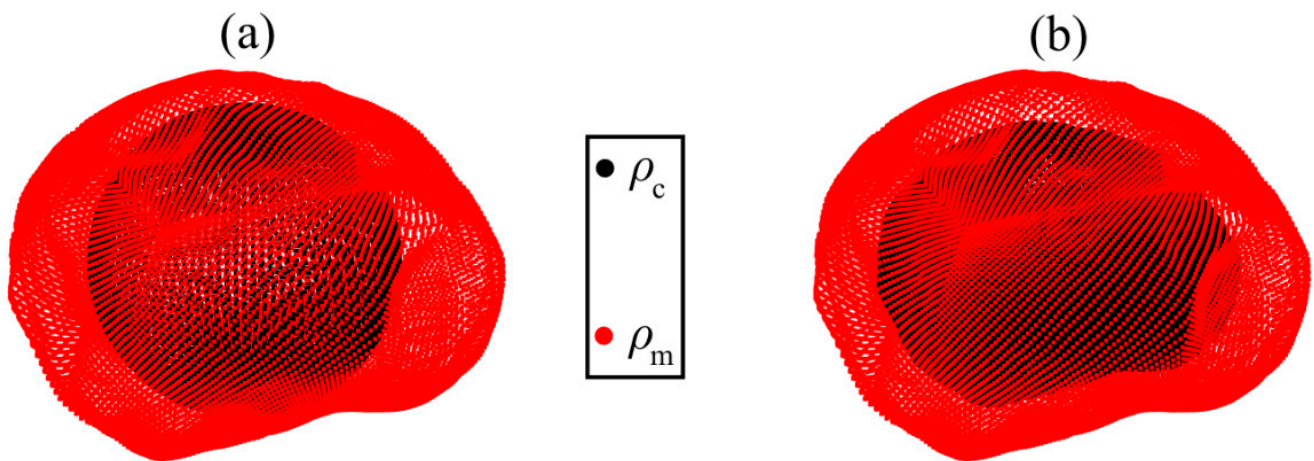


Figure 2. The two-layer model of Phobos. The red shape signifies its irregular outer shape and the black sphere denotes its interior core with a density ρ_c . The area between the red outer shape and the black sphere represents the outer layer with a density ρ_m . (a) shows Model-I with a spherical core that has a radius of r_c close to 8.2 km, and (b) displays Model-II with an irregularly shaped core with a mean radius of r_c close to 8.2 km. The shape of the core shown in subfigure (b) resembles the surface of Phobos.

3. Theory and Method

To explore the interior structure, it is needed to derive the moment of inertia with respect to gravity coefficients. According to previous studies [13,27,29], we can obtain the relations as follows:

$$\frac{A}{MR^2} = \frac{I}{MR^2} + \frac{C_{2,0}}{3} + 2C_{2,2}, \quad \frac{B}{MR^2} = \frac{I}{MR^2} + \frac{C_{2,0}}{3} - 2C_{2,2}$$

$$\frac{C}{MR^2} = \frac{I}{MR^2} - \frac{2C_{2,0}}{3}, \quad I = \frac{A + B + C}{3} \tag{1}$$

where A , B , and C are the main moments of inertia with $A \leq B \leq C$, and their mean value is represented by I . M and R represent the mass and the mean radius of Phobos, respectively. $C_{2,0}$ and $C_{2,2}$ denote the unnormalized gravity coefficients of degree-2, which were provided by recent studies [19]. Even with only Equation (1), it is yet impossible to determine the mean moment of inertia. The relative moment of inertia γ can be considered, which is associated with the forced libration amplitude θ_A . According to the study of Willner et al. [10], the relations are written as follows:

$$\gamma = \frac{B - A}{C}, \quad \gamma = \frac{1}{3\left(1 - \frac{2e}{\theta_A}\right)} \tag{2}$$

where e represents the orbital eccentricity of Phobos. The related parameters are shown in Table 1. According to Equations (1) and (2), the derived mean moment of inertia factor I/MR^2 is written as follows:

$$\frac{I}{MR^2} = \frac{2}{3}C_{2,0} + 12C_{2,2}\left(1 - \frac{2e}{\theta_A}\right) \tag{3}$$

To detect the likely structure, we also need to calculate the modeled moment of inertia I_{mod} as well as the modeled bulk density $\bar{\rho}_{\text{mod}}$ of Phobos. For Model-I in Figure 2a, we can derive the expression as follows:

$$I_{\text{mod}} = \rho_m \int_0^\pi \int_0^{2\pi} \int_0^{r_p} r^4 \sin^3 \theta dr d\phi d\theta - \rho_m \int_0^\pi \int_0^{2\pi} \int_0^{r_c} r^4 \sin^3 \theta dr d\phi d\theta + \rho_c \int_0^\pi \int_0^{2\pi} \int_0^{r_c} r^4 \sin^3 \theta dr d\phi d\theta \tag{4}$$

$$\bar{\rho}_{\text{mod}} = \rho_m + (\rho_c - \rho_m) \frac{4\pi r_c^3}{3V} \tag{5}$$

where r_p is the radius of a certain point on the surface of Phobos. θ and ϕ denote the colatitude and longitude of the point. The expression for Model-II in Figure 2b can be written as follows:

$$I_{\text{mod}} = \rho_m \int_0^\pi \int_0^{2\pi} \int_0^{r_p} r^4 \sin^3 \theta dr d\phi d\theta - \rho_m \int_0^\pi \int_0^{2\pi} \int_0^{\frac{r_c}{R} r_p} r^4 \sin^3 \theta dr d\phi d\theta + \rho_c \int_0^\pi \int_0^{2\pi} \int_0^{\frac{r_c}{R} r_p} r^4 \sin^3 \theta dr d\phi d\theta \tag{6}$$

$$\bar{\rho}_{\text{mod}} = \rho_m + (\rho_c - \rho_m) \left(\frac{r_c}{R}\right)^3 \tag{7}$$

Table 1. Values of the related parameters of Phobos.

Number	Parameters	Values
1	Mass M [19]	$(1.060261 \pm 0.001124) \times 10^{16}$ kg
2	Volume V [1]	5742 ± 35 km ³
3	Mean radius R [1]	~11.1 km
4	Mean density $\bar{\rho}$ [19]	1846 ± 11 kg·m ⁻³
5	Orbital eccentricity e [30]	0.01511°
6	Libration amplitude θ_A	$-1.09^\circ \pm 0.10^\circ$ observed by Oberst et al. [31]
		$-1.143^\circ \pm 0.025^\circ$ observed by Burmeister et al. [12]
7	Unnormalized gravity coefficients of degree-2 [19]	$C_{2,0} = -0.1378 \pm 0.0348,$
		$C_{2,2} = 0.0166 \pm 0.0153$
8	Core radius r_c	0–10 km
9	Core density ρ_c	1000–3000 kg·m ⁻³
10	The outer layer density ρ_m	1000–3000 kg·m ⁻³

It can be found that the estimation of I_{mod} in Equations (4) and (6) can be quite complex due to the integrals. Regarding specific values of ρ_m and ρ_c , they remain constant and can be extracted directly from the integrals. We can first store the integral for certain densities. Here, we calculate the integral with Phobos mean density $\bar{\rho}$ as follows:

$$I_0 = \bar{\rho} \int_0^\pi \int_0^{2\pi} \int_0^{r_p} r^4 \sin^3 \theta dr d\phi d\theta \tag{8}$$

Then, Equations (4) and (6) can be written as follows:

$$I_{\text{mod}} = \frac{\rho_m}{\bar{\rho}} I_0 + (\rho_c - \rho_m) \frac{8}{15} \pi r_c^5 \tag{9}$$

$$I_{\text{mod}} = \left[\frac{\rho_m}{\bar{\rho}} + \frac{\rho_c - \rho_m}{\bar{\rho}} \left(\frac{r_c}{R} \right)^5 \right] I_0 \quad (10)$$

Considering Equations (5)–(10), we used the joint inversion of mean density and mean moment of inertia to calculate the misfit function f as follows:

$$f = \sqrt{(\bar{\rho}_{\text{mod}} - \bar{\rho})^2 + (I_{\text{mod}} - I)^2} \quad (11)$$

The appropriate parameters can be found by minimizing the misfit values according to Equation (11). Using Equations (5)–(11), the influence of the estimated parameter x on the misfit function f can be assessed according to the sensitivity function $S(f, x)$, which is written as follows:

$$S(f, x) = \frac{\Delta f / f}{\Delta x / x} = \frac{\partial f}{\partial x} \frac{x}{f} \quad (12)$$

The estimated parameter x includes the core radius r_c , the core density ρ_c , and the outer layer density ρ_m . The best values for these parameters are those that result in misfit values close to zero, as a close-to-zero misfit indicates a good fit between the model and observed data. In cases where there is noise in the measured parameters, it may not be possible to achieve misfit values close to zero. In this situation, a threshold value of $f < 0.1$ was used as the inversion condition. The frequency distribution of these parameters can provide useful information about their optimized values [15,16].

To constrain the interior structure of Phobos, the estimated parameters (e.g., r_c , ρ_c , and ρ_m) were sampled using an equal probability distribution. The frequency distribution of these parameters was obtained using the same threshold $f < 0.1$. By analyzing the frequency distribution, the interior structure of Phobos can be better understood and constrained. It is important to note that Equation (8) is nonlinear, which can make parameter estimation challenging. The particle swarm optimization (PSO) method simulates the social behavior of birds, bees, or schools of fish, and performs well in solving nonlinear problems with multiple parameters [32]. We considered the PSO method to estimate the optimized parameters of Phobos.

4. Results

For Model-I shown in Figure 2a, utilizes Equations (3), (5), (9), and (11) to estimate optimized parameters through a joint inversion of mean density and mean moment of inertia. Similarly, Equations (3), (7), (10), and (11) were considered to perform the inversion for Model-II in Figure 2b. Our study involved multiple experiments and comparisons, which showed that the frequency distribution of more than 1500 particles remained consistent. We further tested the case of more than 1000 iterations and confirmed that the resulting frequency distribution was the same as the case of 1000 iterations. We thus considered the PSO method with a population size of 1500 particles and 1000 iterations in our study. To ensure the stability of the frequency distribution, the PSO calculation was performed close to 10,000 times. By repeating the PSO calculation multiple times to reduce the impact of random noise on the results, we can obtain a more reliable estimation for the optimized parameters.

We used the fixed values in Table 1 to calculate the moment of inertia by using Equation (3), and obtained the frequency distribution of different parameters. The libration amplitudes provided by Oberst et al. [31] and Lainey et al. [11] are capable of generating normally distributed parameters, while the libration amplitudes provided by Burmeister et al. [11] cannot. The outcomes derived from the libration amplitudes provided by Oberst et al. [31] and Lainey et al. [11] are comparable due to the similar values of libration amplitudes. Therefore, we present the outcomes obtained by using the libration amplitudes provided by Lainey et al. [11] in Figures 3 and 4.

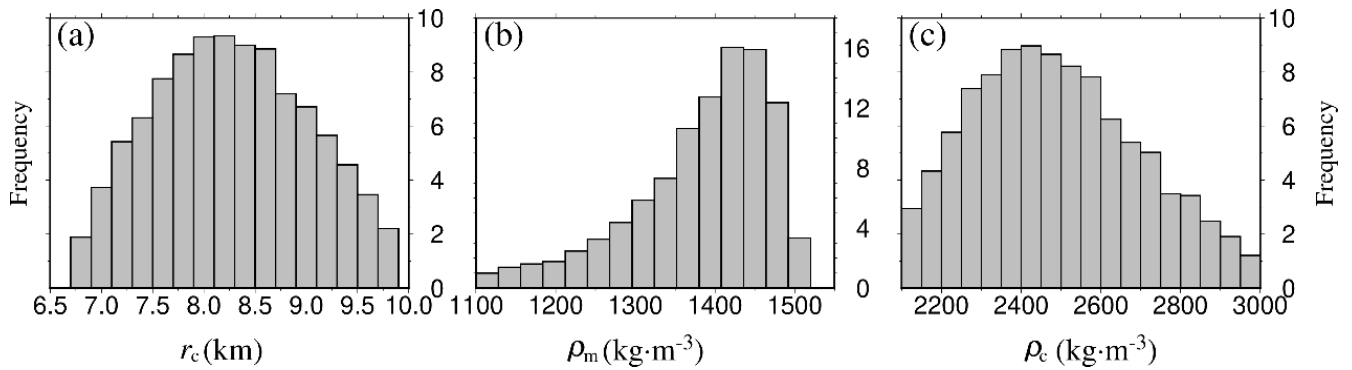


Figure 3. Frequency distribution of Model-I. (a) shows the frequency distribution for the core radius, (b) displays the frequency distribution for the core density, and (c) exhibits the frequency distribution for the density of the outer layer.

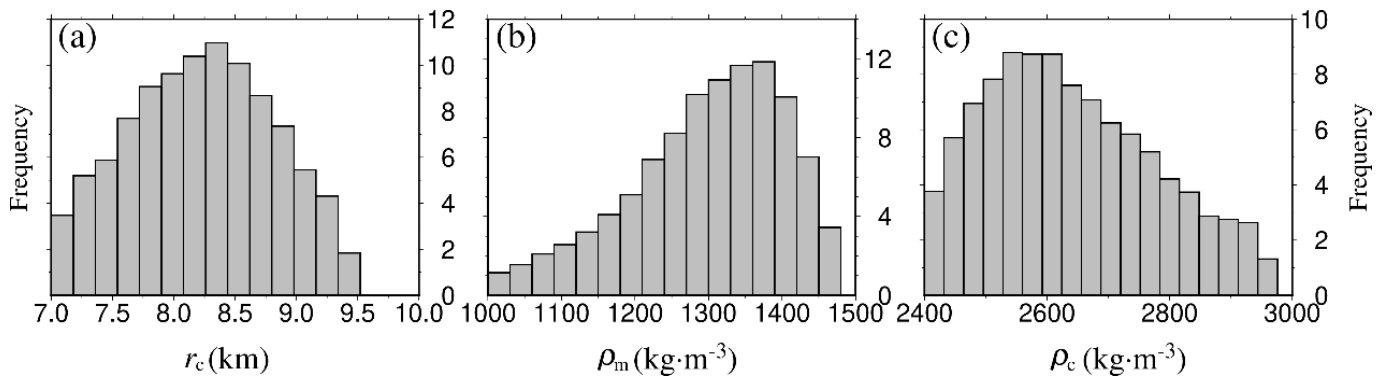


Figure 4. Frequency distribution of Model-II. (a) shows the frequency distribution for the core radius, (b) displays the frequency distribution for the core density, and (c) exhibits the frequency distribution for the density of the outer layer.

Figures 3 and 4 describe the frequency distributions of various parameters for the two models, Model-I and Model-II. In Figures 3a and 4a, the core radius r_c is the parameter being analyzed. It is found that the radius mainly centers around 8.2 km and fluctuates from approximately 7 to 10 km. Figures 3b and 4b display the frequency distributions for the outer-layer density, denoted as ρ_m . In Figure 3b, the density ranges from 1127 to 1452 $\text{kg}\cdot\text{m}^{-3}$, with an optimized value of 1439 $\text{kg}\cdot\text{m}^{-3}$. Meanwhile, in Figure 4b, the density ranges from 1000 to 1427 $\text{kg}\cdot\text{m}^{-3}$, with a likely value of 1340 $\text{kg}\cdot\text{m}^{-3}$. The core density in Figure 3c centers around 2423 $\text{kg}\cdot\text{m}^{-3}$, varying from 2127 to 2985 $\text{kg}\cdot\text{m}^{-3}$. Figure 4c indicated that the core density is between 2425 and 2990 $\text{kg}\cdot\text{m}^{-3}$, with an optimized value near 2573 $\text{kg}\cdot\text{m}^{-3}$. These estimated parameters are also listed in Table 2.

Table 2. The optimized parameters inversed for Phobos and their sensitivities to the misfit function.

Target	r_c (km)	ρ_m ($\text{kg}\cdot\text{m}^{-3}$)	ρ_c ($\text{kg}\cdot\text{m}^{-3}$)
Estimated parameters for Model-I	$8.2^{+1.7}_{-1.3}$	1439^{+75}_{-339}	2423^{+562}_{-296}
Estimated parameters for Model-II	$8.2^{+1.1}_{-1.0}$	1340^{+87}_{-340}	2573^{+417}_{-148}
Sensitivities $S_1(f, x)$ of various optimized parameters for Model-I	-4.6	-6.2	-2.3
Sensitivities $S_2(f, x)$ of various optimized parameters for Model-II	-5.8	-4.5	-2.4

If the estimated parameters are not sensitive to the misfit function, their optimized values will be meaningless. Therefore, we used Equation (12) to estimate the sensitivities for these estimated parameters based on the optimized values listed in Table 2. The results indicate that changes in the parameters could affect the misfit function, with a sensitivity of approximately -4.6 for the core radius for Model-I and -5.8 for Model-II. The outer layer density also has a sensitivity of around -6.2 for Model-I and close to -4.5 for Model-II. Both models have similar sensitivities for the core density, with values of -2.3 for Model-I and -2.4 for Model-II. Additionally, the core density has the lowest absolute value of sensitivity among all the parameters. However, a 1% increase in core density for Model-II would decrease the sensitivity of $S_2(f, \rho_c)$ by 2.4%. Overall, the estimated parameters are sensitive to changes in the misfit function. These inversed parameters are thus reliable in this study.

5. Discussion

Based on the optimized parameters in Table 1, we proposed a set of estimated parameter values. The core of Phobos is likely to have a size of approximately 8.2 km with a corresponding density of around $2500 \text{ kg}\cdot\text{m}^{-3}$. Additionally, the remaining density of the outer layer is close to $1400 \text{ kg}\cdot\text{m}^{-3}$. Our results nearly agree with a previous study by Willner et al. [10], in which they constructed a two-layer model with a 5 km thick outer layer with a density of $1600 \text{ kg}\cdot\text{m}^{-3}$ and found the remaining core with a bulk density close to $2800 \text{ kg}\cdot\text{m}^{-3}$. Our results also indicate a similar distribution of increased density as the model proposed by Dmitrovskii et al. [14], which presents two possible scenarios: one with a positive density gradient, and the other with discrete layers exhibiting increasing density with depth. In addition, even though the study of Guo et al. [21] demonstrated that Phobos' core density was lower than that of its outer layer, they also discovered instances where the core density ($\rho_c = 2200 \text{ kg}\cdot\text{m}^{-3}$) was greater than that the outer layer ($\rho_m = 1810 \text{ kg}\cdot\text{m}^{-3}$). Our findings suggest that an increasing interior density with depth is a likely configuration for Phobos.

Regarding the origin of Phobos, a giant impact [33,34] resulting in primitive ring-moon recycling evolution [35] has been proposed. The water ice content is likely related to the process of re-accretion. Using the optimized radius and densities in this study, we speculated the fractional water ice content. It should be noted that the densities of the core and outer layer represent the average values for the corresponding layers. Moreover, they are the bulk densities for the respective layers. The regolith density of Phobos was observed to be approximately $1600 \text{ kg}\cdot\text{m}^{-3}$ [36], but the thickness of the regolith remains undetermined [21]. The numerical study demonstrated the regolith thickness to be close to tens of kilometers [20]. Considering that our models indicate an outer layer thickness of approximately 3 km and the regolith was formed due to small-impact erosion followed by re-accretion, it is likely that the rock density in the outer layer exceeds the observed regolith density of $1600 \text{ kg}\cdot\text{m}^{-3}$. Assuming an outer layer porosity of 30% [37] and a density of $930 \text{ kg}\cdot\text{m}^{-3}$ for water ice, we used a potential rock density of $2200 \text{ kg}\cdot\text{m}^{-3}$ to estimate the fractional water ice content, which was found to be approximately 11%. The mean value of rock density and the estimated content of water ice are close to previous studies [38,39]. Additionally, we used the potential rock density of carbonaceous compositions ($\sim 3000 \text{ kg}\cdot\text{m}^{-3}$) and a lower porosity of 15% than the outer layer to estimate the water ice content in the core. It was found that the fractional water ice content is around 2.4%, which is significantly lower than that of the outer layer. This result shows that the distribution of bulk density aligns with the likely formation of Phobos, providing a valuable reference for examining the interior structure of small bodies with irregular shapes.

6. Conclusions

The interior structure of Phobos has been a topic of debate in recent years, with the moment of inertia playing a crucial role in determining the density distribution inside the

moon. New gravity coefficients of degree-2 were derived for Phobos from MEX Doppler-tracking data, along with updated forced libration amplitudes. Using the low-degree coefficients of gravity and the forced libration amplitudes, we determined the moment of inertia for Phobos. Before estimating its interior structure, two models with a two-layer interior structure were introduced, one consisting of a spherical core (Model-I) and another with an irregularly shaped surface similar to Phobos' surface (Model-II). The estimated parameters for these models included the core radius r_c , the core density ρ_c , and the density ρ_m of the outer layer. Based on these parameters, we derived the modeled moment of inertia and mean densities for the two models.

To speculate on the potential structure of Phobos, we considered the estimated parameters to be normally distributed and employed a joint inversion of mean density and mean moment of inertia using the PSO method. By minimizing the misfit between the derived and modeled moment of inertia as well as the observed and modeled mean density of Phobos, we obtained the frequency distribution for the estimated parameters. The results showed that the optimized radius of the core was around 8.2 km for both models, with a compromised core density of approximately $2500 \text{ kg}\cdot\text{m}^{-3}$ and an outer layer density of around $1400 \text{ kg}\cdot\text{m}^{-3}$.

We also tested the sensitivity of the estimated parameters on the misfit function and found that they were reliable. Finally, using the compromised values, we speculated on the possible water ice content of Phobos. The results indicated a fractional water ice content in the outer layer of approximately 11% with a rock density of $2200 \text{ kg}\cdot\text{m}^{-3}$, while the content in the core was lower at 2.4% with a rock density of $3000 \text{ kg}\cdot\text{m}^{-3}$. Compared with previous studies of similar methods, our methodology takes into account the irregular shape of celestial bodies. Consequently, our models are more suitable for estimating the internal structure of small celestial bodies by leveraging the mean moment of inertia and mean density. This work can serve as a reference for constraining the interior structure of irregularly shaped asteroids.

Author Contributions: Conceptualization, Z.Z.; Methodology, Z.Z.; Investigation, L.P.; Data curation, Q.W.; Writing—original draft, Z.Z.; Writing—review & editing, Z.Z. and J.Y. supervision, project administration, and funding acquisition, J.Y. All authors have read and agreed to the published version of the manuscript.

Funding: This research was supported by the National Natural Science Foundation of China under Grants 42030110 and 41874010.

Data Availability Statement: The shape model of Phobos is available at https://pds-geosciences.wustl.edu/mex/mex-msa-hrsc-5-refdr-phobos-maps-v1/mexhrs_5001/data/dtm/, accessed on 19 April 2023.

Acknowledgments: The authors would like to thank the PDS project, which provided the shape model of Phobos.

Conflicts of Interest: The authors declare no conflict of interest.

References

1. Willner, K.; Shi, X.; Oberst, J. Phobos' shape and topography models. *Planet. Space Sci.* **2014**, *102*, 51–59. [CrossRef]
2. Schmedemann, N.; Kneissl, T.; Ivanov, B.A.; Michael, G.G.; Wagner, R.J.; Neukum, G.; Ruesch, O.; Hiesinger, H.; Krohn, K.; Roatsch, T.; et al. The cratering record, chronology and surface ages of (4) Vesta in comparison to smaller asteroids and the ages of HED meteorites. *Planet. Space Sci.* **2014**, *103*, 104–130. [CrossRef]
3. Syal, M.B.; Rovny, J.; Owen, J.M.; Miller, P. Excavating Stickney crater at Phobos. *Geophys. Res. Lett.* **2016**, *43*, 595–601.
4. Matsumoto, K.; Hirata, N.; Ikeda, H.; Kouyama, T.; Senshu, H.; Yamamoto, K.; Noda, H.; Miyamoto, H.; Araya, A.; Araki, H.; et al. MMX geodesy investigations: Science requirements and observation strategy. *Earth Planets Space* **2021**, *73*, 226. [CrossRef]
5. Poggiali, G.; Matsuoka, M.; Barucci, M.A.; Brucato, J.R.; Beck, P.; Fornasier, S.; Doressoundiram, A.; Merlin, F.; Alberini, A. Phobos and Deimos surface composition: Search for spectroscopic analogues Get access Arrow. *Mon. Not. R. Astron. Soc.* **2022**, *516*, 465–476. [CrossRef]
6. Hesselbrock, A.J.; Minton, D.A. An ongoing satellite–ring cycle of Mars and the origins of Phobos and Deimos. *Nat. Geosci.* **2017**, *10*, 266–269. [CrossRef]

7. Usui, T.; Bajo, K.; Fujiya, W.; Furukawa, Y.; Koike, M.; Miura, Y.N.; Sugahara, H.; Tachibana, S.; Takano, Y.; Kuramoto, K. The Importance of Phobos Sample Return for Understanding the Mars-Moon System. *Space Sci. Rev.* **2020**, *216*, 49. [[CrossRef](#)]
8. Kuramoto, K.; Kawakatsu, Y.; Fujimoto, M.; Araya, A.; Barucci, M.A.; Genda, H.; Hirata, N.; Ikeda, H.; Imamura, T.; Helbert, J.; et al. Martian moons exploration MMX: Sample return mission to Phobos elucidating formation processes of habitable planets. *Earth Planets Space* **2022**, *74*, 12. [[CrossRef](#)]
9. Duxbury, T.C. The figure of Phobos. *Icarus* **1989**, *78*, 169–180. [[CrossRef](#)]
10. Willner, K.; Oberst, J.; Hussmann, H.; Giese, B.; Hoffmann, H.; Matz, K.D.; Roatsch, T.; Duxbury, T. Phobos control point network, rotation, and shape. *Earth Planet. Sc. Lett.* **2010**, *294*, 541–546. [[CrossRef](#)]
11. Lainey, V.; Pasewaldt, A.; Robert, V.; Rosenblatt, P.; Jaumann, R.; Oberst, J.; Roatsch, T.; Willner, K.; Ziese, R.; Thuillot, W. Mars moon ephemerides after 14 years of Mars Express data. *Astron. Astrophys.* **2021**, *650*, A64. [[CrossRef](#)]
12. Burmeister, S.; Willner, K.; Schmidt, V.; Oberst, J. Determination of Phobos' rotational parameters by an inertial frame bundle block adjustment. *J. Geodesy.* **2018**, *92*, 963–973. [[CrossRef](#)]
13. Le Maistre, S.; Rivoldini, A.; Rosenblatt, P. Signature of Phobos' interior structure in its gravity field and libration. *Icarus* **2019**, *321*, 272–290. [[CrossRef](#)]
14. Dmitrovskii, A.A.; Khan, A.; Boehm, C.; Bagheri, A.; Driel, M.V.C. Constraints on the interior structure of Phobos from tidal deformation modeling. *Icarus* **2022**, *372*, 114714. [[CrossRef](#)]
15. Sohl, F.; Schubert, G.; Spohn, T. Geophysical constraints on the composition and structure of the Martian interior. *J. Geophys. Res. Planet.* **2005**, *110*, E12008. [[CrossRef](#)]
16. Yan, J.; Xu, L.; Li, F.; Matsumoto, K.; Rodriguez, J.A.P.; Miyamoto, H.; Dohm, J.M. Lunar core structure investigation: Implication of GRAIL gravity field model. *Adv. Space Res.* **2015**, *55*, 1721–1727. [[CrossRef](#)]
17. Kahan, D.S.; Folkner, W.M.; Buccino, D.R.; Dehant, V.; Le Maistre, S.; Rivoldini, A.; Van Hoolst, T.; Yseboodt, M.; Marty, J.C. Mars precession rate determined from radiometric tracking of the Insight Lander. *Planet. Space Sci.* **2021**, *199*, 105208. [[CrossRef](#)]
18. Zhong, Z.; Wen, Q.; Liang, J. Constraining the size and density composition of the Martian core by using second-order potential coefficient and recent precession rate of gravity field model. *Acta Phys. Sin.* **2023**, *72*, 029601. [[CrossRef](#)]
19. Yang, X.; Yan, J.G.; Andert, T.; Ye, M.; Pätzold, M.; Hahn, M.; Jin, W.T.; Li, F.; Barriot, J.P. The second-degree gravity coefficients of Phobos from two Mars Express flybys. *Mon. Not. R. Astron. Soc.* **2019**, *490*, 2007–2012. [[CrossRef](#)]
20. Beitz, E.; Blum, J.; Parisi, M.G.; Trigo-Rodríguez, J. The collisional evolution of undifferentiated asteroids and the formation of chondritic meteoroids. *Astrophys. J.* **2016**, *824*, 12. [[CrossRef](#)]
21. Guo, X.; Yan, J.; Andert, T.; Yang, X.; Pätzold, M.; Hahn, M.; Ye, M.; Liu, S.; Li, F.; Barriot, J.P. A lighter core for Phobos? *Astron. Astrophys.* **2021**, *651*, A110. [[CrossRef](#)]
22. Thomas, P.C. The shapes of small satellites. *Icarus* **1989**, *77*, 248–274. [[CrossRef](#)]
23. Simonelli, D.P.; Thomas, P.C.; Carcich, B.T.; Veverka, J. The generation and use of numerical shape models for irregular solar system objects. *Icarus* **1993**, *103*, 49–61. [[CrossRef](#)]
24. Wang, Y.; Wu, X. Analysis of Phobos' dynamical environment considering effects of ephemerides and physical libration. *Mon. Not. R. Astron. Soc.* **2020**, *497*, 416–434. [[CrossRef](#)]
25. Mueller, N.; Piqueux, S.; Lemmon, M.; Maki, J.; Lorenz, R.D.; Grott, M.; Spohn, T.; Smrekar, S.E.; Knollenberg, J.; Hudson, T.L.; et al. Near Surface Properties of Martian Regolith Derived From InSight HP3-RAD Temperature Observations During Phobos Transits. *Geophys. Res. Lett.* **2021**, *48*, e2021GL093542. [[CrossRef](#)]
26. Available online: https://pds-geosciences.wustl.edu/mex/mex-msa-hrsc-5-refdr-phobos-maps-v1/mexhrs_5001/data/dtm/ (accessed on 19 April 2023).
27. Bagheri, A.; Khan, A.; Efroimsky, M.; Giardini, D. Dynamical evidence for Phobos and Deimos as remnants of a disrupted common progenitor. *Nat. Astron.* **2021**, *5*, 539–543. [[CrossRef](#)]
28. Guo, X.; Yan, J.G.; Yang, X.; Liu, L.; Chen, Y.H.; Barriot, J.P. Simulation of Phobos gravity field estimation from Tianwen-1 flybys and implications for the modelling of Phobos' internal structure. *Mon. Not. R. Astron. Soc.* **2023**, *520*, 925–934. [[CrossRef](#)]
29. Rambaux, N.; Castillo-Rogez, J.C.; Le Maistre, S.; Rosenblatt, P. Rotational motion of Phobos. *Astron. Astrophys.* **2012**, *548*, A14. [[CrossRef](#)]
30. Jacobson, R.A. The orbits and masses of the Martian satellites and the libration of Phobos. *Astron. J.* **2010**, *139*, 668. [[CrossRef](#)]
31. Oberst, J.; Zubarev, A.; Nadezhdina, I.; Shishkina, L.; Rambaux, N. The Phobos geodetic control point network and rotation model. *Planet. Space Sci.* **2014**, *102*, 45–50. [[CrossRef](#)]
32. Zhong, Z.; Yan, J.; Jin, S.; Zhu, M.; Rodriguez, J.A.P.; Zhu, H.; Li, Y. Selenophysical parameter inversion in the Lunar Southern Hemisphere Highland based on mutant particle swarm optimization. *Phys. Earth Planet. In.* **2019**, *292*, 55–66. [[CrossRef](#)]
33. Rosenblatt, P.; Charnoz, S.; Dunseath, K.M.; Terao-Dunseath, M.; Trinh, A.; Hyodo, R.; Genda, H.; Toupin, S. Accretion of Phobos and Deimos in an extended debris disc stirred by transient moons. *Nat. Geosci.* **2016**, *9*, 581–583. [[CrossRef](#)]
34. Canup, R.; Salmon, J. Origin of Phobos and Deimos by the impact of a Vesta-to-Ceres sized body with Mars. *Sci. Adv.* **2018**, *4*, eaar6887. [[CrossRef](#)] [[PubMed](#)]
35. Ćuk, M.; Minton, D.A.; Pouplin, J.L.L.; Wishard, C. Evidence for a Past Martian Ring from the Orbital Inclination of Deimos. *Astrophys. J. Lett.* **2020**, *896*, L28. [[CrossRef](#)]
36. Busch, M.W.; Ostro, S.J.; Benner, L.A.M.; Giorgini, J.D.; Magri, C.; Howell, E.S.; Nolan, M.C.; Hine, A.A.; Campbell, D.B.; Shapiro, I.I.; et al. Arecibo radar observations of Phobos and Deimos. *Icarus* **2007**, *186*, 581–584. [[CrossRef](#)]

37. Pätzold, M.; Andert, T.P.; Tyler, G.L.; Asmar, S.W.; Häusler, B.; Tellmann, S. Phobos mass determination from the very close flyby of Mars Express in 2010. *Icarus* **2014**, *229*, 92–98. [[CrossRef](#)]
38. Macke, R.J.; Consolmagno, G.J.; Britt, D.T. Density, porosity, and magnetic susceptibility of carbonaceous chondrites. *Meteorit. Planet. Sci.* **2011**, *46*, 1842–1862. [[CrossRef](#)]
39. Trigo-Rodríguez, J.M.; Rimola, A.; Tanbakouei, S.; Soto, V.C.; Lee, M. Accretion of water in carbonaceous chondrites: Current evidence and implications for the delivery of water to early Earth. *Space Sci. Rev.* **2019**, *215*, 18. [[CrossRef](#)]

Disclaimer/Publisher’s Note: The statements, opinions and data contained in all publications are solely those of the individual author(s) and contributor(s) and not of MDPI and/or the editor(s). MDPI and/or the editor(s) disclaim responsibility for any injury to people or property resulting from any ideas, methods, instructions or products referred to in the content.